

Studying exothermic reactions in the Ni-Al system at rapid heating rates using a nanocalorimeter

P. Swaminathan, M. D. Grapes, K. Woll, S. C. Barron, D. A. LaVan, and T. P. Weihs

Citation: [Journal of Applied Physics](#) **113**, 143509 (2013); doi: 10.1063/1.4799628

View online: <http://dx.doi.org/10.1063/1.4799628>

View Table of Contents: <http://scitation.aip.org/content/aip/journal/jap/113/14?ver=pdfcov>

Published by the [AIP Publishing](#)

Articles you may be interested in

[Investigation on structural instability induced relaxation and crystallization in ZrCuAlNi bulk metallic glass](#)
J. Appl. Phys. **112**, 083530 (2012); 10.1063/1.4762013

[Magnetostructural phase transitions and magnetocaloric effects in MnNiGe_{1-x}Al_x](#)
Appl. Phys. Lett. **100**, 052404 (2012); 10.1063/1.3681798

[In situ observation of rapid reactions in nanoscale Ni-Al multilayer foils using synchrotron radiation](#)
Appl. Phys. Lett. **97**, 144101 (2010); 10.1063/1.3485673

[Thermodynamic study of the temperature memory effects in Cu-Al-Ni shape memory alloys](#)
J. Appl. Phys. **107**, 083518 (2010); 10.1063/1.3357310

[Quantitative Landau potentials for the martensitic transformation in Ni-Al](#)
Appl. Phys. Lett. **90**, 221903 (2007); 10.1063/1.2743927



Studying exothermic reactions in the Ni-Al system at rapid heating rates using a nanocalorimeter

P. Swaminathan,^{1,2,a)} M. D. Grapes,¹ K. Woll,¹ S. C. Barron,^{1,2} D. A. LaVan,^{2,b)} and T. P. Weihs¹

¹Department of Materials Science and Engineering, Johns Hopkins University, Baltimore, Maryland 21218, USA

²Functional Properties Group, Materials Measurement Science Division, Material Measurement Laboratory, National Institute of Standards and Technology, Gaithersburg, Maryland 20899, USA

(Received 3 February 2013; accepted 21 March 2013; published online 10 April 2013)

Heats of reaction and heat capacity changes were measured using scanning nanocalorimetry for a nickel and aluminum bilayer where initial heating rates of 10^4 K/s were achieved. Multiple exotherms were observed on the initial heating, but the number of intermediate exotherms decreased with increasing heating rate. The final phase was the B2 NiAl intermetallic. Results from the nanocalorimeter were compared with a conventional differential scanning calorimeter (operating at 0.7 K/s) to understand the effect of significant ($10\,000\times$) increases in heating rate on the phase transformation sequence. The high heating rate in the nanocalorimeter delays reaction initiation, causes the exothermic peaks to shift to higher temperatures, and appears to suppress the formation of intermediate, metastable phases. Potential explanations for this apparent suppression are discussed. © 2013 American Institute of Physics. [<http://dx.doi.org/10.1063/1.4799628>]

I. INTRODUCTION

Reactive multilayers consist of alternating layers of metals or alloys that react exothermically to form intermetallics.^{1,2} The thicknesses of the individual layers range from a few nm to a few μm and are formed by vapor deposition of alternate layers of materials.³ Other production methods include stacking and rolling many micron thick, individual foils into laminates⁴ and ball-milling of particles.⁵ In these cases, the average reactant spacing is on the order of μm 's (Ref. 4) or nm's (Ref. 5) and is not as well defined as in vapor deposition. Reactive multilayers can be used as local heat sources for the bonding of large components with mismatches in thermal expansion coefficients and for the joining of temperature-sensitive electronic materials.^{6,7} By adjusting the composition, the individual layer thicknesses, and the total thickness of the materials it is possible to obtain a self-propagating reaction through the multilayer foils.^{1,3,8} In self-propagation, the energy released from the reaction zone heats the material in front of it causing the material to react and the process proceeds along the foil. Multilayers can also be ignited in a uniform manner where the entire foil is heated above a critical temperature that causes a spontaneous reaction to occur.⁹

Layered thin films have also served as model materials for studying solid-state reactions in binary metallic systems. The reaction sequence, activation energies, and the kinetics and thermodynamics of reactions in multilayers have been investigated by a variety of techniques. A typical practice uses a conventional differential scanning calorimeter (DSC) to measure the energy stored in the materials and an *ex situ* structure characterization technique like X-ray diffraction

(XRD) to investigate the phase transformation sequence¹⁰ that appears during the DSC scans. For 1:1 Ni:Al multilayers, DSC measurements at 0.7 K/s show that the final B2 NiAl phase forms through a series of metastable intermetallics, progressively richer in Ni. While most reactions have been characterized in the solid state at slow heating rates, some have been examined at very rapid heating rates using self-propagating reactions. *In situ* experiments of self-propagating reactions have confirmed that most atomic mixing occurs in the liquid state and products nucleate from the resulting liquid solutions. These studies use *in-situ* x-ray diffraction¹¹ or electron diffraction^{12,13} to characterize the sequence of phase transformations that appear during self-propagating reactions with heating rates as high as 10^7 K/s. For example, the formation of a liquid phase has been observed in Ni-Al multilayer foils that enable rapid mixing of Ni and Al in the liquid state and direct precipitation of the B2 NiAl phase from the melt.^{11–13} Similarly, high heating rates can shift the formation temperatures of intermediate phases, and the steep concentration gradients that appear in multilayer materials may alter the reaction sequence.^{14–16} However, measuring enthalpy changes at high rates (10^4 K/s– 10^6 K/s) is challenging.

Here, we use nanocalorimeters to study rapid exothermic solid-state reactions in the Ni-Al multilayer system; specifically we characterize the effect of heating rates on the temperature and the number of exothermic reactions, which are correlated with particular formation reactions. The nanocalorimeters are prepared using standard microfabrication methods and their small mass enables measurement of heat capacities and enthalpies of reactions in single Ni:Al bilayers at heating rates ranging from 10^3 K/s to 10^5 K/s.^{17,18} The high heating rates shift the exothermic peaks to higher temperatures, as compared to peaks in DSC scans of much thicker samples with similar chemistries and bilayer thicknesses. By comparing peaks from both slow and fast heating

^{a)}swamnthn@gmail.com

^{b)}david.lavan@nist.gov

rate experiments, we provide indirect evidence that rapid heating suppresses the formation of intermediate phases and we propose possible theoretical explanations.

II. EXPERIMENTAL DETAILS

Thick Ni:Al multilayer foils for DSC measurements were prepared by DC magnetron sputtering from commercially pure Al and a Ni – 7% V target. V was included in the Ni to suppress its magnetism for ease of sputtering. The foils were deposited onto a water-cooled brass substrate, which rotated between the sputtering targets, resulting in alternating layers of Ni and Al. Four different Ni:Al bilayers, 23 nm, 58 nm, 93 nm, and 150 nm, were deposited and the bilayer thicknesses (measured from the center of one Ni layer to the center of the next Ni layer) were controlled by the rotation speed and the power applied to the targets. The total thickness of each foil was approximately 10 μm (thus each foil contained hundreds of bilayers). The enthalpies of reaction for the foils were measured by twice heating samples in a Perkin Elmer DSC from 323 K to 998 K at 40 K/min (0.7 K/s) in flowing Ar gas and by integrating the net power curves.¹⁰ For each bilayer spacing, the data were averaged from four samples. To characterize the intermediate phases, additional first scans were interrupted by quenching from specific temperatures and the phases present were characterized *ex situ* using XRD and Cu K α radiation.

For the nanocalorimeter experiments, Ni:Al bilayers were deposited onto the SiN_x side of a nanocalorimeter chip using e-beam deposition, a custom designed shadow mask, and pure Al and Ni charges (purity >99% per manufacturers specification). Prior to deposition the resistance vs. temperature profiles of the nanocalorimeter chips were obtained using a pyrometer¹⁹ and the heat capacities of the bare chips were measured. Bilayers of thicknesses 25, 40, 50, and 60 nm were deposited and were capped on both sides by 10 nm thick Al₂O₃ layers. An Al-Ni-Al layer sequence was formed with 2 half-layers of Al sandwiching a full layer of Ni, so that two interfaces exist for mixing. After deposition the reactions were measured in vacuum, with a base pressure of 10⁻⁷ Torr. The measurement consisted of applying current pulses (with pulse duration controlled in the range of tens of ms) through a nanocalorimeter chip containing the sample and a bare chip serving as a reference.²⁰ Three samples of each bilayer thickness were measured at different heating rates obtained by changing the duration of the current pulse between 20 ms and 100 ms. The voltage drop across each sensor and the difference in the voltage drops were measured during reactions at a sampling rate of 100 kHz (every 10 μs) and were converted to temperature from the *a priori* temperature calibration. Final phases were identified post-reaction using electron back scattered diffraction (EBSD) in a Hitachi S-4700 SEM. Cross-sectional samples were also prepared by focused ion beam (FIB) etching using a Zeiss NVision 40 FIB and then imaged in a Philips CM 300 TEM.

III. RESULTS AND DISCUSSION

The sequence of phase transformations and the total amount of heat stored in free-standing multilayer foils can be

probed using conventional DSC, and the results for three bilayer spacings for the 1:1 Ni:Al multilayer foil are shown in Fig. 1. The reactions are irreversible and the final phase formed in all three cases is the B2 NiAl phase. From Fig. 1, it can be seen that the reaction starts around 480 K and the number of troughs increases with increasing bilayer thickness. Each trough corresponds to an exothermic reaction, which can either be the formation of a new phase or the growth of an existing phase.¹⁰ The temperature of the troughs also increases with bilayer spacing. This is due to the increase in bilayer thickness and hence a larger diffusion distance, along with the constant heating rate in the DSC. The integration of the DSC curve yields the total energy stored in the multilayer material. The reaction sequence to form the B2 NiAl phase can be probed by quenching at select intermediate temperatures (based on the DSC scan) and probing the phases present. The reaction sequence for the formation of the NiAl phase in these DSC scans is given by



The sequence is unaltered for increasing bilayer thicknesses, though multiple phases can co-exist during heating of samples with thicker layers, due to simultaneous nucleation of new phases and growth of existing ones (bilayer thicknesses as large as 2 μm were also considered). The above reaction sequence is generally consistent with earlier studies, but others^{11,21,22} have reported that the first intermetallic to nucleate is the nonequilibrium Al₉Ni₂ phase. While we cannot rule out the presence of this phase early in the first exotherm, we can conclusively report the presence of the above metastable phases that are progressively richer in Ni, consistent with fast, asymmetric diffusion of Ni into Al.

In order to study the effect of a higher heating rate on the temperatures, sequences, and enthalpies of the reactions, we make use of the nanocalorimeter. The results from

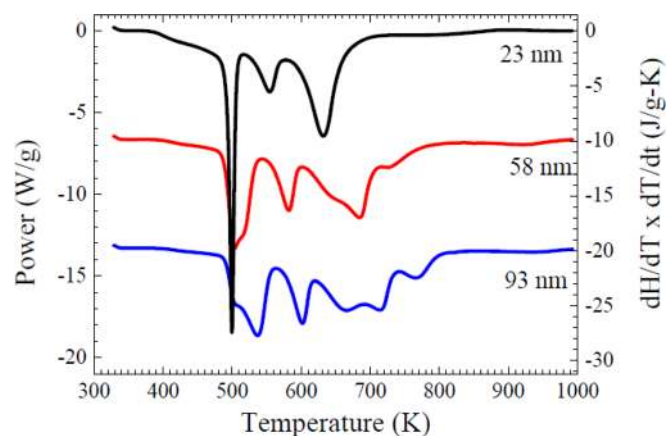


FIG. 1. DSC traces of Ni:Al multilayers for three different bilayer thicknesses (23 nm, 58 nm, and 93 nm). The scans were performed from room temperature to 998 K, at a heating rate of 0.7 K/s and are offset vertically for clarity. The scale on the left corresponds to the power measured in the DSC which can be divided by the constant heating rate and integrated to obtain the heat of reaction. The final phase for all three bilayers was B2 NiAl and quenching and *ex-situ* diffraction shows that the intermediate phases are NiAl₃ and then Ni₂Al₃.

heating a 25 nm bilayer sample in the nanocalorimeter are summarized in Fig. 2. The individual layer thicknesses are 7.5 nm Al, 10 nm Ni, and 7.5 nm Al with 10 nm thick Al_2O_3 layers sandwiching the Al and Ni. The nanocalorimeter chip containing the Ni:Al bilayer and a bare reference chip are heated using a 60 ms current pulse obtained by discharging a capacitor. Inline resistances control the current flowing through the chip and hence the nominal heating rate. Fig. 2(a) shows the temperature vs. time profile for the first and second current pulses on the sample chip. There is a 2 s wait time between pulses for the chip and sample to cool to room temperature. During the first pulse, the Ni and Al reacted exothermically and the heat released causes the chip temperature to increase at a faster rate than it would due simply with the applied current. No exothermic reaction is seen in the second or subsequent pulses, indicating the exothermic reactions are completed in the first pulse. Differentiating the temperature with respect to time gives the heating rate, which is plotted as a function of temperature in Fig. 2(b). The exothermic reactions can be seen as peaks in the heating rate plot.

In Fig. 2(b) three peaks are seen in the plot of heating rate vs. temperature. Similarly, three peaks were observed for samples with 50 nm and 75 nm bilayer thickness heated with a 100 ms and 60 ms pulse, respectively. At higher heating rates for these bilayers, obtained by either increasing the current and/or changing the pulse duration, two peaks are observed. The transition from three to two peaks and the change in the intermediate phase sequence is discussed in detail later for the 25 nm bilayer. An important point to note is that the number of peaks and peak positions depend on

several factors. One is the thickness of the bilayers as noted earlier. A second is the initial heating rate, that is controlled by the pulse time and the current applied to the nanocalorimeter. A third is the heating rate during the exothermic reactions which depends not only on the applied current but also on the volume of the bilayer, heat losses to the surrounding, and the nature of the phase transformations. In this nanocalorimeter, the applied current is discharged from a capacitor without closed-loop control during the experiment; the power released by the sample is also uncontrolled. Thus, the heating rates are not constant during these nanocalorimetry experiments. In addition, they cannot be specified precisely from experiment to experiment. However, the initial heating rates can be increased or decreased by varying the duration of capacitor discharge and current-limiting resistor value; the actual heating rate is recorded for analysis.

For the 25 nm bilayer sample depicted in Fig. 2, the initial heating rate, due to the applied current, is $2 \times 10^4 \text{ K/s}$ with a maximum value of $6.5 \times 10^4 \text{ K/s}$ due to the heat released during the reaction. In the second pulse the heating rate decreases monotonically, due to the increased heat loss at higher temperature. From the applied current and voltage, the power supplied to it can be measured and is assumed to be dissipated as heat. Since the measurements are done in vacuum, heat loss is limited to conduction (to the Si frame) and radiation; the values for these losses are measured *a priori* on the bare chip and on the sample chip, post-reaction.²³ The applied power and the heat loss are plotted in Fig. 2(c) as a function of temperature. The total amount of heat released during reaction can be obtained by the following series of calculations:

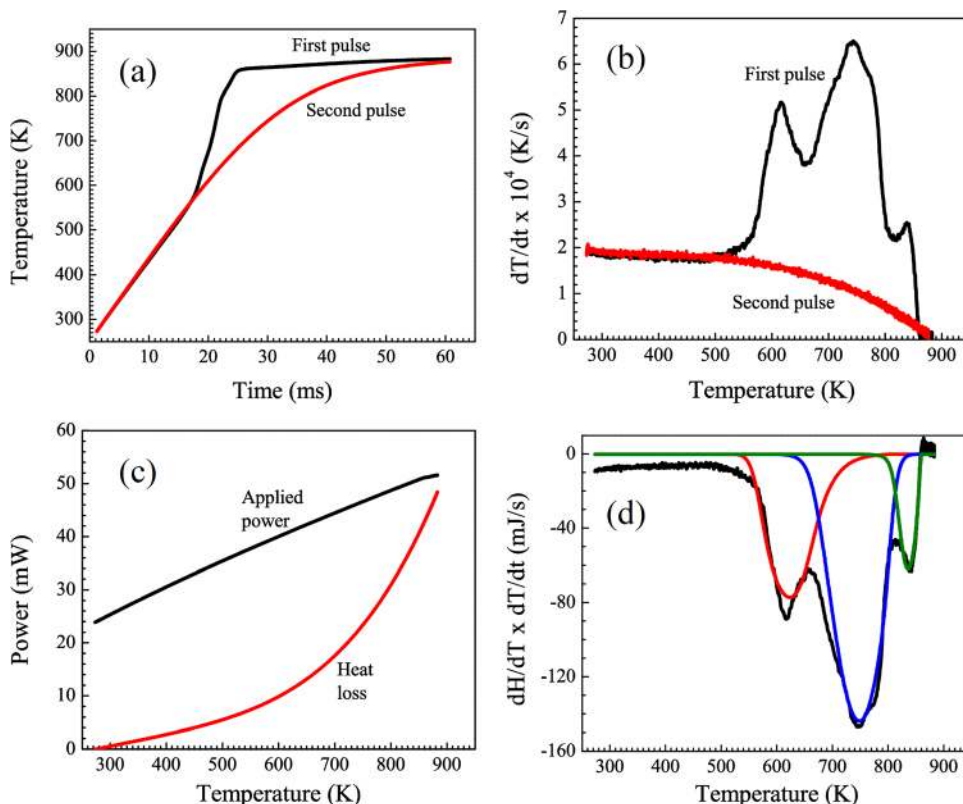


FIG. 2. Nanocalorimeter results for a 25 nm Ni:Al bilayer. (a) Temperature vs. time profile for the first and second heating pulse. The exothermic reaction causes a rapid temperature rise in the first pulse, relative to the first pulse. The reaction is complete by the end of the first pulse since in the second pulse only a monotonic rise is seen due to the externally applied current. (b) Heating rate vs. temperature obtained by differentiating the curves in (a) with respect to time. Three peaks are seen for the first heating pulse corresponding to three exothermic reactions. (c) Applied power and heat loss as a function of temperature for the first pulse. Heat losses are conductive and radiative and are measured on the bare chip before deposition of the Ni:Al bilayer. (d) The reaction rate as a function of temperature, calculated using Eq. (2). The plot also shows Gaussian fits to the three exothermic peaks to determine their positions. The peak positions are listed in Table I.

$$\begin{aligned}
C_p^{chip} &= \frac{P_s - W_L}{dT/dt} \\
C_p^{chip} &= C_p^{barechip} + C_p^{NiAl} + \frac{dH}{dT} \\
\frac{dH}{dT} &= \frac{P_s - W_L}{dT/dt} - (C_p^{barechip} + C_p^{NiAl}) \\
\frac{dH}{dT} \times \frac{dT}{dt} &= (P_s - W_L) - (C_p^{barechip} + C_p^{NiAl}) \times \frac{dT}{dt},
\end{aligned} \quad (2)$$

where P_s is the applied power, W_L is the heat loss, and dT/dt is the heating rate of the chip. C_p^{chip} is the total measured heat capacity, which includes the heat capacity of the Pt and the SiN_x layers ($C_p^{barechip}$), the heat capacity of the Ni, Al, and Al_2O_3 (C_p^{NiAl}) layers and the evolution of the energy stored in the bilayer (dH/dT). $dH/dT \times dT/dt$ vs. temperature is plotted in Fig. 2(d) and mirrors the plot of power vs temperature found in Fig. 1 for a conventional DSC scan. The peak positions in the nanocalorimeter data and the DSC data can be obtained by a Gaussian fit to each trough and are compared in Table I.

The phases identified in Table I are from the quenching experiments of foils heated in the DSC. To ensure that the same final product, B2 NiAl, formed in the first scan in the nanocalorimeter experiments, we investigated the structure of the final phase using cross-sectional TEM and EBSD (Figure 3). The cross-sectional TEM specimen shown in Figure 3 was a 50 nm bilayer sample and it was prepared post-reaction by a standard FIB sample preparation technique.²⁷ The figure also includes EBSD patterns from three different grains along with the best match to the patterns. The cross-sectional TEM image shows a polycrystalline structure with large, nearly through thickness grains, though some smaller grains are also seen. These grain structures are similar to those obtained by multilayer foils heated in a DSC where the grain sizes are similar to a single bilayer thickness.¹¹ On the other hand, grains formed during uncontrolled, self-propagating reactions where maximum temperatures are much higher than the Al melting point are expected to be much larger than the bilayer spacing due to intermixing in the liquid state and precipitation from the melt.¹¹ The best fit to the EBSD patterns in Fig. 3 is the B2 NiAl intermetallic (PDF 65-0420). The three different patterns indicate that the grains are randomly oriented. Grain

TABLE I. Peak temperature comparison between nanocalorimeter scans and DSC scans for a 23 nm Ni:Al multilayer foil and a 25 nm Ni:Al bilayer. The difference in nominal heating rates between the two techniques is 10^4 K/s. The DSC peaks are obtained from Gaussian fits to the data in Fig. 1, while the peaks from the nanocalorimeter are obtained from the fits in Fig. 2(d). The four orders of magnitude higher heating rate in the nanocalorimeter causes the peaks to shift to higher temperatures than the DSC. The peak shifts calculated using Eq. (3) are also tabulated and are within 5% of the measured value.

Peak number	Phase	DSC			Nanocalorimeter	
		Measured (K)	Measured (K)	Predicted (K)	Measured (K)	Predicted (K)
1	Al_3Ni	499	624	650	624	650
2	Al_3Ni_2	556	749	783	749	783
3	AlNi	631	836	846	836	846

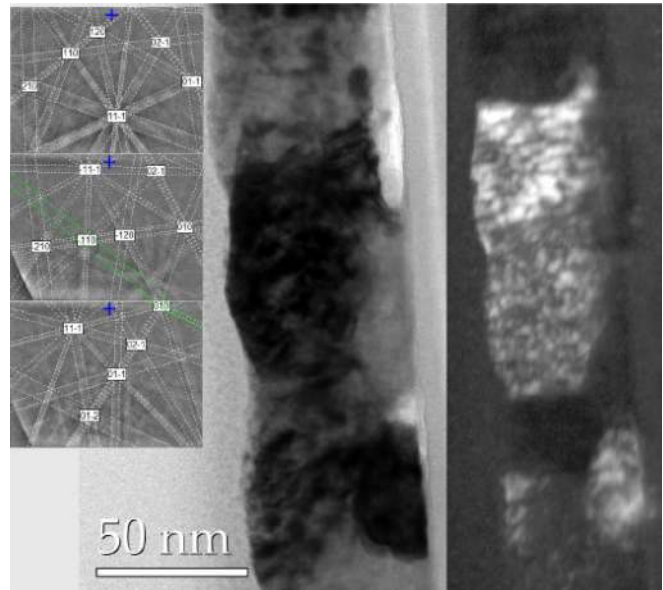


FIG. 3. Bright field and corresponding dark field cross-sectional TEM images from a 50 nm Ni:Al bilayer that was reacted completely on the nanocalorimeter. The cross-sectional images were obtained by focused ion beam processing of the nanocalorimeter sample and show large, through thickness grains with varying orientations. The inset to the figure shows electron backscattered diffraction patterns from a reacted 50 nm Ni:Al bilayer. The best match to the patterns is 1:1 NiAl B2 intermetallic (PDF 65-0420), which is shown as a series of dotted lines superimposed on the EBSD patterns. Other bilayers also show the NiAl B2 intermetallic phase following heating. For the different bilayers the reaction proceeds to completion in one heating pulse and subsequent pulses do not show any exothermic peaks corresponding to phase formation.

sizes measured from plan view images in the SEM are of the order of the bilayer thickness and agree with the cross sectional images. The combination of EBSD and cross-sectional TEM leads us to conclude that the reactions in the nanocalorimeter proceeded to completion in the solid state in the first pulse and formed the final B2 NiAl phase. These conclusions are true for other bilayers as well. The reaction proceeded to completion within the first pulse and subsequent pulses did not show reaction peaks.

Knowing both sets of samples react to form the same final phase, we now consider the shift in peak temperatures shown in Table I that arise as the heating rate increases four orders of magnitude on going from the DSC studies to the nanocalorimeter experiments. A Kissinger analysis has been used to calculate average activation energies of the Ni_xAl_y formation reactions based on the shift of the exotherms with higher heating rates. Using reported activation energies for the formation of NiAl_3 (1.9 eV),²¹ Ni_2Al_3 (1.7 eV),²¹ and NiAl (2.2 eV),⁴ and the nominal heating rate in the nanocalorimeter (2×10^4 K/s), we can also predict the shifts in the peak positions using the same Kissinger analysis¹⁰

$$\frac{\beta_1 T_1}{\beta_2 T_2} = \exp\left(\frac{E_d}{k_B} \left(\frac{1}{T_2} - \frac{1}{T_1}\right)\right), \quad (3)$$

where β_1 and β_2 are the heating rates in the nanocalorimeter and DSC, respectively, and T_1 and T_2 are the corresponding peak positions, E_d is the activation energy, and k_B is the Boltzmann constant. (Note: While the initial heating rate is

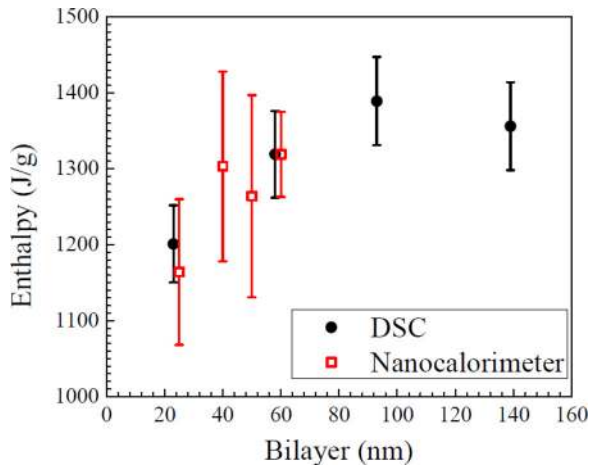


FIG. 4. Plot of heats of reaction measured using Ni:Al bilayer samples and the nanocalorimeter and Ni:Al multilayer samples and a conventional DSC. Error bars represent the mean plus and minus one standard deviation. For the DSC measurements $N = 4$, with the same heating rate. For the nanocalorimeter $N = 3$, with different heating rates.

2×10^4 K/s in the nanocalorimeter scan in Fig. 2, it increases to a maximum value of 6.5×10^4 K/s during the reaction for reasons noted above.) For the Kissinger analysis, the initial heating rate of 2×10^4 K/s was used. The peak positions predicted using Eq. (3) are listed in Table I. The calculated values are within 5% of the measured exotherm peaks in the nanocalorimeter. Thus, a simple Kissinger analysis can be used to understand the shift in peak position at increased heating rates assuming the same sequence of phase transformations.

The power data in Fig. 2(d) can be integrated to obtain the total amount of heat released during the reaction in the nanocalorimeter. Similarly, the power data in the DSC curves can also be used to calculate the energy released from the multilayer foils. These heats of reaction are plotted as a function of bilayer thickness in Fig. 4. Note that both sets of heats of reaction increase with bilayer thickness and then the DSC data approaches a constant value as reported earlier for multiple multilayer systems.^{10,21} The variation is related to the percentage of the bilayer that is intermixed during deposition. Assuming the amount of intermixing is relatively constant for a given deposition process, the percentage of heat that is lost due to intermixing during deposition decreases as thicker layers are deposited and the intermixing becomes a smaller fraction of the total multilayer volume. This trend is seen in the heats of reaction obtained from the DSC samples

with hundreds of bilayers; it is also seen in the heats of reaction measured using single bilayers on nanocalorimeters. The maximum expected heat of reaction for the nanocalorimeter samples is simply the enthalpy of formation for NiAl, 59 kJ/mol atom or 1390 J/g.²⁴ For the DSC foils, though, formed by sputtering with Ni – 7% V, previous studies report a maximum heat of reaction of approximately 1300 J/g.^{25,26} The heats of reaction obtained from our DSC scans for large bilayer samples are approximately 7% higher than 1300 J/g, but slight variations in chemistry could account for these difference. The heats of reaction obtained from the nanocalorimetry studies are within the standard deviations of the DSC values. For example, the 25 nm DSC samples yielded a heat of reaction equal to 1201 J/g \pm 51 J/g (mean with standard deviation from 4 samples), while the 25 nm nanocalorimeter samples yielded 1164 J/g \pm 96 J/g (mean with standard deviation from 3 samples). This suggests that the nanocalorimetry measurements are a reliable means to quantify the heats of reaction, even at the very high heating rates. However, experiments for a broader range of bilayer thicknesses and larger bilayers in particular will be needed to effectively predict a maximum heat of reaction in the single bilayer samples.

As noted earlier, the high heating rate in the nanocalorimeter can influence the phase sequence by increasing the nucleation temperatures; it may also suppress the formation of intermediate phases. In order to test this hypothesis, we heated two nanocalorimeter chips with 25 nm Ni:Al bilayer samples with initial rates of 2×10^4 K/s and 3.3×10^4 K/s. The heating rate was varied by changing the duration and current of the heating pulse. The results of these experiments are summarized in Fig. 5, as a plot of heating rate and enthalpy of reaction vs. temperature; the peak positions for the two experiments are summarized in Table II. At the higher heating rate, the number of exothermic peaks decreases to 2 from 3, however, in both cases, no further exothermic peaks were observed for subsequent current pulses indicating that the reaction proceeded to completion in the first cycle. To understand this apparent disappearance of an exothermic reaction, we first consider an earlier report of shifts in peak positions with heating rate.

Blobaum *et al.* studied the effect of increasing heating rate on the position of the DSC peaks for the Ni-Al system.²¹ The heating rates in their study varied from 0.083 K/s to 1.67 K/s, which produced a peak shift of 40 K for a 50 nm

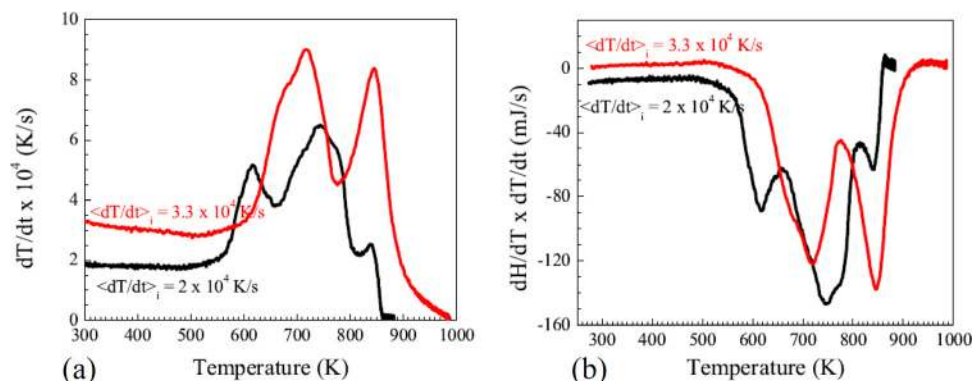


FIG. 5. (a) Effect of the heating rate on the number of exothermic peaks for a 25 nm Ni:Al bilayer measured using a nanocalorimeter. For an initial heating rate of 2×10^4 K/s there are 3 peaks in the exotherm (same as Fig. 2(d)), but an increase in the initial heating rate to 3.3×10^4 K/s decreases the number of peaks to 2. The increased heating rate appears to suppress nucleation of an intermediate phase due to the steeper concentration gradient. (b) The plot of heating rate vs. temperature in (a) is converted to enthalpy vs. temperature using Eq. (2).

TABLE II. Peak position comparison for a 25 nm Ni:Al bilayer heated in the nanocalorimeter at two different heating rates. For the lower heating rate (2×10^4 K/s) three exotherms are seen while for the higher heating rate (3.3×10^4 K/s) only 2 exotherms are observed. The table also includes the positions of the peaks for the higher heating rates predicted using Eq. (3) and the peaks for the lower heating rate.

Peak number	Peak position (K)		
	$(dT/dt = 2 \times 10^4 \text{ K/s})$		$(dT/dt = 3.3 \times 10^4 \text{ K/s})$
	Measured	Calculated	Measured
1	624	632.8	...
2	749	763.4	706.0
3	836	847.8	847

2Ni:3Al bilayer. The increase in heating rate, however, did not change the sequence of the intermediate phases that formed. In a similar manner, we have measured and predicted shifts in peak positions in the nanocalorimeter due to increases in heating rate from 2×10^4 K/s to 3.3×10^4 K/s. The three peaks at the lower heating rate were measured to be 624 K, 749 K, and 836 K and these were predicted to shift modestly to 634 K, 763 K, and 848 K at the higher heating rate using Eq. (3). We begin a comparison of predicted and measured temperatures for the higher heating rate by considering the last exotherm first.

Note that the final, measured peak temperature at the higher heating rate (3.3×10^4 K/s) matches the predicted value very well, with only a 1 K difference. This suggests that the final exotherm in both experiments corresponds to the same transformation to the final phase, the B2 intermetallic, NiAl. A similar match, though, is not seen for the first exotherm at the higher heating rate. A likely scenario is that the nucleation of NiAl₃ is skipped and the Ni₂Al₃ intermetallic or a nonequilibrium phase such as an amorphous or a BCC solid solution forms first. The peak for this transformation (706 K) lies in between the first 2 peaks (634 K and 763 K) at the lower heating rates. The final or second exotherm is then simply the transformation of the Ni₂Al₃ phase and excess Ni (or a nonequilibrium phase) to the stable NiAl intermetallic. Next, we consider several theories regarding nucleation to understand how higher heating rates may impact the formation of the first phase.

A variety of theories and models have been suggested to explain and predict the phase selection during the early stages of phase transformations in multilayers under slow heating (≤ 1 K/s). The empirical modeling of Pretorius *et al.* uses the thermodynamic parameters of equilibrium intermetallics to calculate their effective heats of formation.²⁸ The phase with the most negative effective heat of formation, at the concentration of the lowest eutectic in the equilibrium diagram, is predicted to form first. The model effectively predicts the sequence of metastable phases in several Al-based systems. Another theory was proposed by Gösele and Tu.²⁹ They suggest that phase selection can be explained by a competition in the growth of the equilibrium phases that may exist, and they introduce the concept of interfacial reaction barriers to explain their argument. Additionally, Thompson notes that interdiffusion across the Ni/Al (or A/B)

interface is required prior to nucleation³⁰ and can impact which phase forms first. Lastly, Coffey *et al.* provided experimental evidence and a theoretical explanation that the nucleation and growth of the first intermetallic phase can occur in two distinct exotherms under slow heating conditions.³¹

Other researchers, such as Desre and Yavari³² and Gusak,³³ have taken a more fundamental approach to predict nucleation by accounting for the sharp concentration gradients that exist in multilayer films. Using thermodynamic parameters, they calculate phase-specific critical concentration gradients, and they argue that nucleation is enabled once the concentration gradient present at a given phase composition is less than the critical value for that phase. Since the initial concentration gradients in multilayer samples are expected to exceed the critical ones, a retardation of nucleation is anticipated. Gusak *et al.*³⁴ predict that a thermodynamic induction time is required to reduce the concentration gradient by interdiffusion across the A/B interface. Here, we use this model of critical concentration gradients to predict which phase forms first in the DSC and nanocalorimetry experiments as a function of heating rate. While a limited description of the analysis is offered here, a more comprehensive description will be presented in a forthcoming paper.³⁵ The model assumes a cubic nucleus of width $2 \cdot r$ in a concentration gradient, ∇c , and it assumes the gradient is constant within the nucleus volume. The change in the free energy ΔG due to nucleation is calculated by³²⁻³⁴

$$\Delta G = 24\gamma \cdot r^2 + 4\rho\Delta G_{A/B \rightarrow AB} \cdot r^3 + \frac{4}{3} \cdot \alpha \cdot (\nabla^2 c) \cdot r^5. \quad (4)$$

The first two components on the right-hand side represent the interfacial and volumetric contributions according to classical nucleation theory. γ and ρ denote the interfacial energy at the nucleus/parent phase interface and the nucleus density, respectively. $\Delta G_{A/B \rightarrow AB}$ characterizes the maximum driving force for the AB transformation from the elements A and B. The third component denotes the effect of the gradient contribution. α is a constant which depends on the nucleation mode, which can be positive or negative, and is determined by the stability functions of the compound and parent phases. Hodaj and Desre³⁶ and Desre¹⁴ calculated positive α 's for the limiting cases of polymorphic and transversal transformation modes. The former mode describes nucleation without compositional changes. The latter describes nucleation where compositional redistribution occurs perpendicular to the concentration gradient within the nucleus.

The analysis for a given mode of nucleation, whether transversal or polymorphous, has three steps. The first step is a numerical simulation of the intermixing at the interface that predicts the composition profile for some specific time and heating rate. We assume symmetric, bulk diffusion and use Fick's 2nd law to solve for composition profiles in a 25 nm bilayer sample after heating over the range of 400 K to 800 K at different rates. An activation energy of 84 kJ/mol and a frequency factor of $5.18 \cdot 10^{-9}$ m/s² (Ref. 37) describe the temperature dependence of the interdiffusivity. The resulting composition profiles were then used to determine concentration gradients $\nabla c(\text{Ni}_x\text{Al}_y)$ at the compositions

associated with individual compounds, as a function of temperature. In the second step, we calculate the critical concentration gradients $\nabla_c(\text{Ni}_x\text{Al}_y)$ for each possible phase as a function of temperature, according to Eq. (4). The thermodynamic properties of the individual Ni_xAl_y phases are modeled according to Ref. 38 for these calculations, and both transversal and polymorphic nucleation are considered. In the third and final step, we determine the temperature and the first phase for which the local gradient drops below the critical value for a given phase

$$\nabla_c(\text{Ni}_x\text{Al}_y) \leq \nabla_c(\text{Ni}_x\text{Al}_y), \quad (5)$$

thereby, identifying the first phase to nucleate. We now consider two cases in the analysis of nucleation.

Case A: Nucleation with compositional redistribution (transversal mode)

Under slow heating conditions in a DSC, we assume there is sufficient time for chemical redistribution as a nucleus forms. Thus, this case adopts a transversal mode of nucleation that was proposed by Desre,¹⁴ in predicting the first phase to form in the DSC experiments. For comparison, we also assume this mode of nucleation remains effective as heating rate increases up to 2×10^4 K/s. Figure 6(a) shows the temperature evolution of the calculated critical concentration gradients assuming a transversal mode (Eq. (4)); it also displays the numerically predicted concentration gradients for heating rates of 0.7 K/s and 2×10^4 K/s. Note that NiAl_3 reaches the condition for nucleation (Eq. (5)) before Ni_2Al_3 and NiAl , thus predicting it to nucleate first for both heating rates. In fact, NiAl_3 is predicted to nucleate first in the transversal mode, regardless of heating rate, even for a rate of 3.3×10^4 K/s. However, as the heating rate increases, the time for chemical redistribution during the formation of a nucleus decreases and the assumption of a transversal mode of nucleation is likely invalid. At the highest heating rates, we expect limited diffusional mixing during the formation of a nucleus and a polymorphous mode of nucleation. Such a mode is considered in case B.

Case B: Nucleation without compositional redistribution (polymorphic mode)

Figure 6(b) plots the calculated critical concentration gradients for the polymorphic mode of nucleation and the numerically predicted concentration gradients for the high heating rates of 2×10^4 K/s and 3.3×10^4 K/s. Multiple equilibrium phases are considered: NiAl_3 , Ni_2Al_3 , and NiAl . In addition, because of the very high heating rates and the limited time for nucleation at any given temperature, this case also considers a metastable BCC solid solution of Ni and Al (Refs. 34, 39–41) following the related reports from Greer and Assadi and Cantor and Cahn. Greer and Assadi observed the suppression of ordering in intermetallics and the formation of solid solutions during rapid solidification,⁴² and Cantor and Cahn reported the formation of a BCC solid solution in co-deposited Ni-Al thin films.⁴³

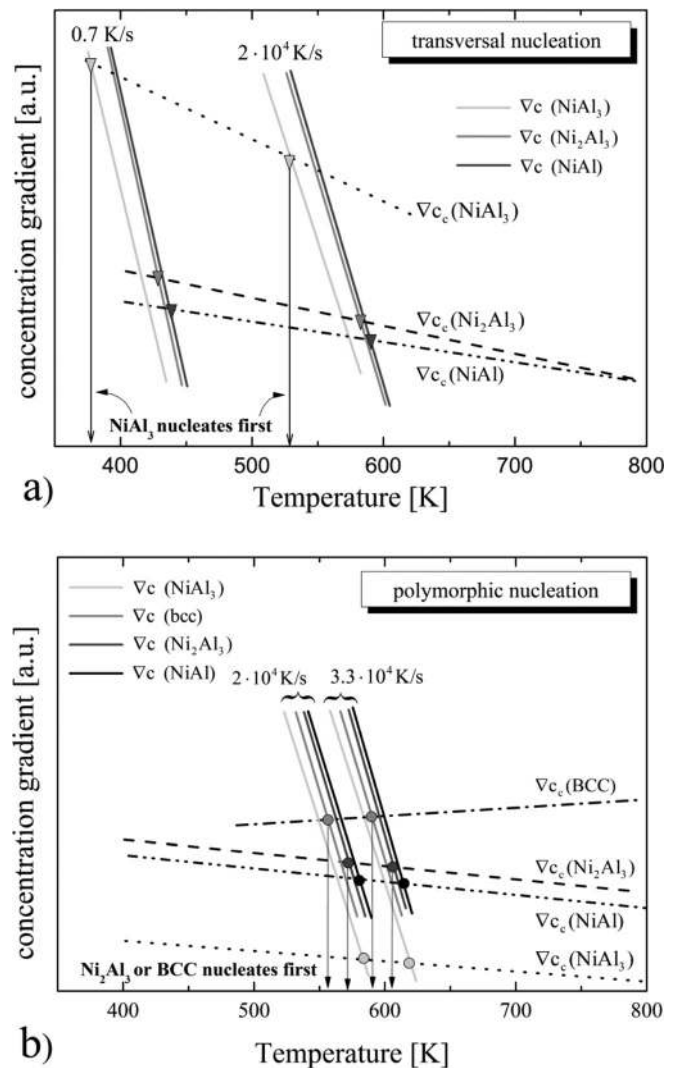


FIG. 6. Plot of the critical concentration gradients ∇_c (dashed lines) obtained using Eq. (4) for (a) transversal and (b) polymorphic nucleation and the numerically simulated concentration gradients ∇_c (solid lines) at the individual compound compositions. In (a) ∇_c 's are calculated for a typical DSC heating rate of 0.7 K/s and the lower heating rate of $2 \cdot 10^4$ K/s of the present study. In (b) ∇_c 's are shown for the heating rates of $2 \cdot 10^4$ K/s and $3.3 \cdot 10^4$ K/s. The nucleation temperatures that are predicted for the intermetallic phases using Eq. (4) are indicated by (a) triangles and (b) circles. The first forming phase is determined by the lowest nucleation temperature.

Three observations are worth noting for Figure 6(b). One is that the critical concentration gradients for the equilibrium phases shift to lower values and the nucleation temperatures shift to higher values compared to the transversal mode of nucleation. We attribute these shifts to the lack of chemical redistribution in the polymorphous analysis and the corresponding impediment to nucleation. Second, note that NiAl_3 is no longer the first phase to form. Instead, the first phase is predicted to be a BCC solid solution or the Ni_2Al_3 intermetallic. Finally, this prediction of which phase forms first does not change with heating rate, even for much slower or much faster values than those presented here. Thus, we are left to suggest that the apparent change in which phase forms first in the 25 nm bilayer samples, as heating rate increases from 2×10^4 K/s to 3.3×10^4 K/s, is caused by a change in nucleation mode from transversal to polymorphic. For slower heating

rates (from the heating rates used in a conventional DSC up to heating rates of 2×10^4 K/s seen in the nanocalorimeter) the assumption of a transversal mode of nucleation predicts that NiAl₃ forms first while for faster heating rates the assumption of a polymorphous mode of nucleation predicts that a BCC solid solution or the Ni₂Al₃ intermetallic forms first. However, we cannot determine conclusively whether the Ni₂Al₃ intermetallic, the BCC solid solution, or some other metastable phase nucleates first. Additional nanocalorimeter studies, with *in situ* microstructural observations, are needed to verify the sequence of phase formation during rapid heating. To this end, experiments are underway to place a nanocalorimeter within a dynamic TEM^{12,13} to study these transformations *in situ* at different heating rates. These experimental results will create a basis for developing a comprehensive model of phase formation in the Ni-Al system at rapid heating rates.³⁵

IV. CONCLUSION

We have studied exothermic reactions in Ni:Al multilayers using a DSC and a nanocalorimeter. The nanocalorimeter has the ability to track enthalpy changes with temperature and thereby obtain heat of reactions at heating rates on the order of 10^4 K/s. The large heat losses of the system and its large heat capacity relative to the Ni:Al bilayer keep the temperature below the melting point of Al so that the reaction occurs in the solid state. The high heating rates enabled by the nanocalorimeter shift the exothermic peaks to substantially higher temperatures compared to the conventional DSC, and these shifts can be predicted using the Kissinger model. With increasing heating rate the number of exothermic peaks is reduced to two from three and the shift in temperatures recorded for those two peaks suggest that the sequence of metastable phase transformations has changed. A possible scenario is that Ni and Al mix to first form a BCC solid solution or the Ni₂Al₃ intermetallic at the highest heating rate instead of the NiAl₃ phase that is known to form first at very low heating rates. This hypothesis is supported by the theory of nucleation within steep concentration gradients and the assumption that local chemical redistribution diminishes during the formation of a nucleus as heating rate increases. Future work will focus on integrating the nanocalorimeter into a dynamic TEM to enable identification of these rapid phase transformations.

ACKNOWLEDGMENTS

Research was supported by NIST Grant No. 70NANB9H9146. Research is performed in part at the NIST Center for Nanoscale Science & Technology. Certain commercial equipment, instruments, or materials are identified in this document. Such identification does not imply recommendation or endorsement by the National Institute of Standards and Technology, nor does it imply that the products identified are necessarily the best available for the purpose. We thank Mark Vaudin at NIST for help with the EBSD measurements and Dr. Kenneth J. T. Livi at the HRAEM Facility of the Integrated Imaging Center at Johns Hopkins University for performing the TEM characterization. The modeling work of

KW was supported by the U.S. DOE Department of Energy, Office of Basic Energy Sciences, Division of Materials Sciences and Engineering under Award No. DE-SC0002509.

- ¹A. Rogachev, *Russ. Chem. Rev.* **77**, 21 (2008).
- ²K. Morsi, *Mater. Sci. Eng., A* **299**, 1 (2001).
- ³A. Gavens, D. V. Heerden, A. Mann, M. Reiss, and T. Weihs, *J. Appl. Phys.* **87**, 1255 (2000).
- ⁴L. Battezzati, P. Pappaleopore, F. Durbiano, and I. Gallino, *Acta Mater.* **47**, 1901 (1999).
- ⁵E. Dreizin, *Prog. Energy Combust. Sci.* **35**, 141 (2009).
- ⁶J. Wang, E. Besnoin, A. Duckham, S. Spey, M. Reiss, O. Knio, M. Powers, M. Whitener, and T. Weihs, *Appl. Phys. Lett.* **83**, 3987 (2003).
- ⁷J. Trenkle, T. Weihs, and T. Hufnagel, *Scr. Mater.* **58**, 315 (2008).
- ⁸E. Besnoin, S. Cerutti, O. Knio, and T. Weihs, *J. Appl. Phys.* **92**, 5474 (2002).
- ⁹L. Thiers, A. Mukasyan, and A. Varma, *Combust. Flame* **131**, 198 (2002).
- ¹⁰C. Michaelsen, K. Barmak, and T. Weihs, *J. Phys. D* **30**, 3167 (1997).
- ¹¹J. Trenkle, L. Koerner, M. Tate, N. Walker, S. Gruner, T. Weihs, and T. Hufnagel, *J. Appl. Phys.* **107**, 113511 (2010).
- ¹²J. Kim, T. LaGrange, B. Reed, R. Knepper, T. Weihs, N. Browning, and G. Campbell, *Acta Mater.* **59**, 3571 (2011).
- ¹³J. Kim, T. LaGrange, B. Reed, M. Taheri, M. Armstrong, W. King, and G. Campbell, *Science* **321**, 1472 (2008).
- ¹⁴P. J. Desre, *Acta Metall. Mater.* **39**, 2309 (1991).
- ¹⁵F. Hodaj, A. Gusak, and P. Desre, *Philos. Mag. A* **77**, 1471 (1998).
- ¹⁶L. Cook, R. Cavicchi, N. Bassim, S. Eustis, W. Wong-Ng, I. Levin, U. Kattner, C. Campbell, C. Montgomery, W. Egelhoff, and M. Vaudin, *J. Appl. Phys.* **106**, 104909 (2009).
- ¹⁷M. Efremov, E. Olsen, M. Zhang, F. Schiettekatte, Z. Zhang, and L. Allen, *Rev. Sci. Instrum.* **75**, 179 (2004).
- ¹⁸R. Kummamuru, L. Rama, L. Hu, M. Vaudin, M. Efremov, M. Green, D. LaVan, and L. Allen, *Appl. Phys. Lett.* **95**, 181911 (2009).
- ¹⁹P. Swaminathan, B. Burke, A. Holness, B. Wilthan, L. Hanssen, T. Weihs, and D. LaVan, *Thermochim. Acta* **522**, 60 (2011).
- ²⁰M. Efremov, E. Olsen, M. Zhang, S. Lai, F. Schiettekatte, Z. Zhang, and L. Allen, *Thermochim. Acta* **412**, 13 (2004).
- ²¹K. Blobaum, D. van Heerden, A. Gavens, and T. Weihs, *Acta Mater.* **51**, 3871 (2003).
- ²²M. H. da Silva Bassani, J. H. Perepezko, A. S. Edlestein, and R. K. Everett, *Scr. Mater.* **37**, 227 (1997).
- ²³P. Swaminathan, D. LaVan, and T. Weihs, *J. Appl. Phys.* **110**, 113519 (2011).
- ²⁴W. Huang and Y. Chang, *Intermetallics* **6**, 487 (1998).
- ²⁵H. Nathani, J. Wang, and T. Weihs, *J. Appl. Phys.* **101**, 104315 (2007).
- ²⁶R. Knepper, M. Syder, G. Fritz, K. Fisher, O. Knio, and T. Weihs, *J. Appl. Phys.* **105**, 083504 (2009).
- ²⁷L. Giannuzzi and F. Stevie, *Micron* **30**, 197 (1999).
- ²⁸R. Pretorius, A. M. Vredenberg, F. W. Saris, and R. de Reus, *J. Appl. Phys.* **70**, 3636 (1991).
- ²⁹U. Gösele and K. N. Tu, *J. Appl. Phys.* **53**, 3252 (1982).
- ³⁰C. V. Thompson, *J. Mater. Res.* **7**, 367 (1992).
- ³¹K. R. Coffey, L. A. Clevenger, K. Barmak, D. A. Rudman, and C. V. Thompson, *Appl. Phys. Lett.* **55**, 852 (1989).
- ³²P. J. Desre and R. Yavari, *Phys. Rev. Lett.* **64**, 1533 (1990).
- ³³A. M. Gusak, T. V. Zaporozhets, Y. O. Lyashenko, S. V. Kornienko, M. O. Pasichnyy, and A. S. Shirinyan, *Diffusion-controlled solid state reactions* (Wiley-VCH, Hoboken, 2011).
- ³⁴A. M. Gusak, F. Hodaj, and A. O. Bogatyrev, *J. Phys. Condens. Matter* **13**, 2767 (2001).
- ³⁵K. Woll, M. Grapes, P. Swaminathan, and T. P. Weihs, "Modeling solid state nucleation in metallic multilayers using the theory of critical concentration gradient," *Phys. Rev. B* (to be submitted).
- ³⁶F. Hodaj and P. J. Desre, *Acta Mater.* **44**, 4485 (1996).
- ³⁷G. M. Fritz, Ph.D. dissertation, Department of Materials Science and Engineering, Johns Hopkins University, 2011.
- ³⁸I. Ansara, N. Dupin, H. L. Lukas, and B. J. Sundaman, *J. Alloys Compd.* **247**, 20 (1997).
- ³⁹K. F. Kelton, A. L. Greer, and C. V. Thompson, *J. Chem. Phys.* **79**, 6261 (1983).
- ⁴⁰K. F. Kelton, *Mater. Sci. Eng., B* **32**, 145 (1995).
- ⁴¹K. F. Kelton and A. L. Greer, *Nucleation in Condensed Matter* (Pergamon Press, Elsevier, Oxford, United Kingdom, 2010).
- ⁴²A. L. Greer and H. Assadi, *Mater. Sci. Eng. A* **226–228**, 133 (1997).
- ⁴³B. Cantor and R. W. Cahn, *Acta Metall.* **24**, 845 (1976).